Available online at www.sciencedirect.com
SCIENCE DIRECT®
ELSEVIER
International Journal of Mechanical Sciences 47 (2005) 1123–1145
International Journal of MECHANICAL SCIENCES
www.elsevier.com/locate/ijmecsci

A new forming-limit criterion for fracture prediction in a powder forging application

Cheng-Chao Huang, Jung-Ho Cheng*

Department of Mechanical Engineering, National Taiwan University, No. 1 Roosevelt Rd. Sec. 4, Taipei 10617, Taiwan

Received 10 May 2004; received in revised form 30 January 2005; accepted 16 February 2005
Available online 4 May 2005

Abstract

This research investigates the forging limit of sintered compacts by taking into particular consideration the effects of void evolution in the process. A new fracture criterion for a porous medium, which is based on the first principal strain energy density (FPSED), is developed as well. The experiment and the finite element analysis (FEA) have been conducted to examine the process. The material properties of porous compacts are measured by both the uni-axial tension and the compression tests. The finite element model is first verified with the upsetting experiment under different frictional conditions. By applying this new criterion, the fracture upsetting simulation demonstrates much better accuracy than the results derived from the equations proposed by other researchers. The fracture prediction in forging the gear blank is also presented as a practical application to reinforce the reliability of this model. Besides the degradation of the strength, this study specifically shows that voids in the sintered preform exponentially reduce the forging limit.

Keywords: Porous materials; Powder forging; Forming limit; Strain energy density; Void evolution; Fracture criteria; FEA

*Corresponding author. Fax: +886 223 631 755.
E-mail addresses: chengchao@ntu.edu.tw (C.-C. Huang), jhcheng@ntu.edu.tw (J.-H. Cheng).

0020-7403/$ - see front matter © 2005 Elsevier Ltd. All rights reserved.
doi:10.1016/j.ijmecsci.2005.02.014

Nomenclature

$C_{1,2,3}$	critical constants for fully dense media in the subsistent fracture criteria
C_{cr}	critical constant for a fully dense matrix in the new fracture criterion
E	Young's modulus
f	void volume fraction (porosity)
$\dot{f}$	total change of void volume fraction
$\dot{f}_g$	change of growth of existing voids
$\dot{f}_n$	change of nucleation of new voids
$\mathbf{I}$	identity matrix
k	coefficient in the plastic equation for a fully dense matrix
m	material constant in the new fracture criterion
n	strain hardening exponent
$q_{1,2,3}$	material parameters in Gurson–Tvergaard yield criterion
$\mathbf{S}$	deviatoric part of Cauchy stress tensor
U	total strain energy density
$U_{1,2,3}$	strain energy densities on principal axes
$\mathrm{d}\bar{\varepsilon}$	effective strain increment
$\bar{\varepsilon}_f$	effective strain at fracture
$\dot{\boldsymbol{\varepsilon}}^p$	plastic flow of materials
$\bar{\varepsilon}_m^p$	effective plastic strain of a fully dense matrix
$\dot{\bar{\varepsilon}}_m^p$	effective plastic flow of a fully dense matrix
$\varepsilon_{1,2,3}$	principal strains
$\mathrm{d}\varepsilon_{1,2,3}$	principal strain increments
$\varepsilon_{1\mathrm{fract}}$	first (maximum) principal strain at fracture
$\dot{\lambda}$	nonnegative plastic flow multiplier
μ	coefficient of friction
v	Poisson's ratio
ρ_{r_0}	initial relative density of a porous preform
$\boldsymbol{\sigma}$	macroscopic Cauchy stress tensor
$\bar{\sigma}$	von Mises effective stress
σ_{h}	hydrostatic stress
$\sigma_{\mathrm{firstyield}}$	first yield stress of porous materials or a fully dense matrix
σ_y	flow stress of a fully dense matrix
σ^*	largest tensile stress
$\sigma_{1,2,3}$	principal stresses
$\boldsymbol{\Phi}$	potential function

1. Introduction

Powder forging (P/F) combines powder metallurgy (P/M) and forging technology and thus possesses the advantages of both processes that result in both stronger and yet more versatile

products with complicated geometry and arbitrary alloy compositions. Preforms are prepared in various steps that involve powder mixing, compacting, and sintering. As a result, the exact shape of each workpiece is obtained from a final forging procedure. P/F process has been widely applied to the production of commercial components, such as gears, connecting rods, ratchet wheels, etc. This process not only enhances the dimension precision but also improves the loading capability of products. Because of the designable profile of green compacts, P/F technique results in fewer dies, less material waste, and lower tooling costs. Nevertheless, voids in sintered compacts bear a detrimental effect on the mechanical properties, and a fracture may occur in the workpiece as a result of major deformation in the forging process. In consideration of P/F applications, the most important issue is the forming limit of sintered materials.

The workability of materials is the subject of several studies in the metalworking process. To date, a variety of forming-limit criteria have been developed. They can be classified into three categories, which are the stress field, the strain field, and the strain energy density formulation. Based on the concept of the strain energy density, the fracture criteria for a fully dense matrix were proposed by many authors such as Freudenthal [1], Cockcroft and Latham [2], Brozzo et al. [3], Norris et al. [4] and Oyane et al. [5]. Recently, Clift et al. [6], Gouveia et al. [7,8], Wifi et al. [9], Jain et al. [10], and Takuda et al. [11] utilized the published continuum workability criteria in the finite element models to predict fracture in workpieces under different working conditions.

As for the forgeability of porous materials, the stress components were utilized by Abdel-Rahman and El-Sheikh [12] to formulate the workability criterion. The fracture loci of the strain ratio (the tensile strain/the compressive strain) for porous billets were investigated by Downey and Kuhn [13] and Zhang et al. [14]. In addition to these, Tabata and Masaki [15] and Lee and Zhang [16] studied the forging limit of porous preforms via the critical values of the strain energy density, where the formulations resemble the criteria for fully dense media. Further, the fracture models considering the influence of voids were examined by McClintock [17], Roy et al. [18], Sowerby and Chandrasekaran [19], Spitzig et al. [20], and Spitzig [21].

Although a substantial amount of studies have been concentrated on the workability for porous metals, the effects of void variation on the forming limit still elude sweeping exploration. The primary purpose of the present work, therefore, is to study the forgeability of sintered compacts by developing a new fracture criterion to exactly consider the results of void evolution (Fig. 1). This research begins with preparing the porous specimens with metal powder via appropriate P/M approaches. The material properties of powder compacts are measured by both the simple tension and the compression tests, giving attention to the experimental setup. The finite element model associated with the material properties is established as well. Particular emphasis is placed on the verification of the finite element results with the upsetting experiment under different frictional conditions. After evaluating the forming limit of sintered materials, the fracture prediction in forging the gear blank by the verified finite element model is carried out to examine the failure mechanism in the workpiece.

2. Theoretical background

2.1. Yield function for porous media

The plastic theories of porous materials have been widely examined. We present the existed yield function for porous media that are used in this research. Gurson [22,23] proposed a yield

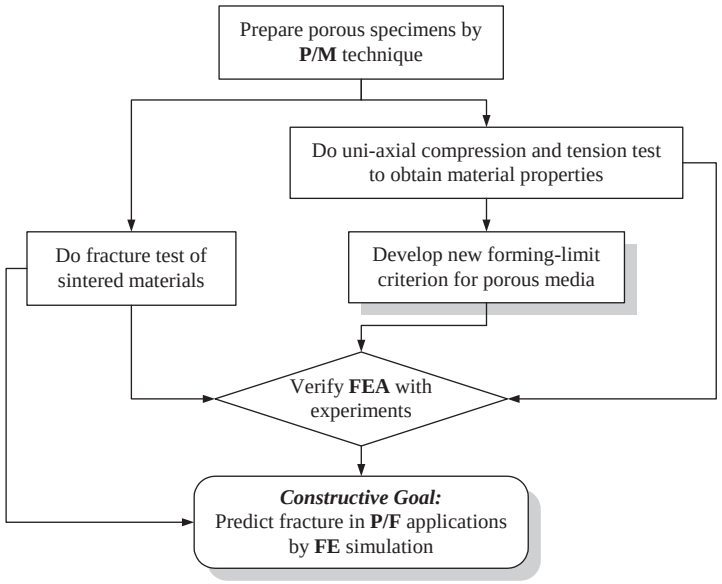

Fig. 1. Flow diagram of this research.

criterion for porous media based on a rigid-plastic upper bound solution for spherical symmetric deformations of a single spherical void in the unit cell. This criterion combines the effects of both the deviatoric part and the hydrostatic component, and is represented as follows:

$$\mathbf{\Phi}(\boldsymbol{\sigma},f)=\left(\frac{\bar{\sigma}}{\sigma_y}\right)^2+2q_1f\,\cosh\left(\frac{3q_2\sigma_h}{2\sigma_y}\right)-(1+q_3f^2)=0, \tag{1}$$

where

$$\bar{\sigma}=\sqrt{\frac{3}{2}\mathbf{S}:\mathbf{S}} \tag{2}$$

is the von Mises effective stress,

$$\mathbf{S}=\boldsymbol{\sigma}-\sigma_h\mathbf{I} \tag{3}$$

is the deviatoric part of the macroscopic Cauchy stress tensor $\boldsymbol{\sigma}$,

$$\sigma_h=\tfrac{1}{3}\boldsymbol{\sigma}:\mathbf{I} \tag{4}$$

is the hydrostatic stress, and $\mathbf{I}$ is the identity matrix; meanwhile, σ_y is the flow stress of a fully dense matrix, f is the void volume fraction, and q_1, q_2, and q_3 are the material parameters. Originally, it was shown that $q_1=q_2=q_3=1$ in Eq. (1). Then, the scalar parameters with $q_1=1.5$, $q_2=1$, and $q_3=q_1^2$ were introduced by Tvergaard [24]. When the porosity is given as zero, $f=0$, Gurson–Tvergaard criterion can be simplified to von Mises formula for the fully dense matrix:

$$\mathbf{\Phi}(\boldsymbol{\sigma})=\bar{\sigma}-\sigma_y=0. \tag{5}$$

2.2. Material constitutive equations

The presence of pressure in the yield conditions results in the nondeviatoric plastic strain. Plastic flow of materials is assumed to be normal to the yield surface

$$\dot{\boldsymbol{\varepsilon}}^p = \dot{\lambda}\frac{\partial \boldsymbol{\Phi}}{\partial \boldsymbol{\sigma}}, \tag{6}$$

where $\dot{\lambda}$ is the nonnegative plastic flow multiplier. The hardening of a fully dense matrix is described with the constitutive equation:

$$\bar{\sigma} = \bar{\sigma}(\bar{\varepsilon}_m^p), \tag{7}$$

where $\bar{\varepsilon}_m^p$ is the effective plastic strain of the matrix. The effective plastic flow of the matrix, $\dot{\bar{\varepsilon}}_m^p$, is obtained from the following effective plastic work expression:

$$(1-f)\sigma_y \dot{\bar{\varepsilon}}_m^p = \boldsymbol{\sigma} : \dot{\boldsymbol{\varepsilon}}^p. \tag{8}$$

2.3. Void evolution

Voids in sintered powder compacts exert a detrimental effect on the mechanical strength and the forming limit. The total change of the void volume fraction in porous metals during deformation arises partly from the growth of existing voids and partly from the nucleation of new voids, a fact that can be stated as

$$\dot{f} = \dot{f}_g + \dot{f}_n, \tag{9}$$

where $\dot{f}_g$ is the growth rate of existing voids and $\dot{f}_n$ is the change of the nucleation of new voids. The growth of existing voids is formulated based on the law of conservation of mass and is expressed as

$$\dot{f}_g = (1-f)\dot{\boldsymbol{\varepsilon}}^p : \mathbf{I}. \tag{10}$$

On the other hand, the nucleation of new voids stems from the grain boundaries or decohesion of the particle–matrix interface in the tensile stress state. Void nucleation at a material point, therefore, will not be considered in the compressive stress state. The mechanisms of void growth and nucleation during the plastic deformation were subsequently reviewed by Goods and Brown [25], Chu and Needleman [26], Hom and McMeeking [27], Lee and Zhang [28], and Yi [29].

3. A new fracture criterion for porous media

3.1. Subsistent workability criteria

The main purpose of the present work is to investigate the forgeability of sintered compacts. Before the development of the new workability criterion, we analyze the equations that have been proposed. Several fracture criteria for a fully dense matrix or porous metals, expressed by the strain energy density, are demonstrated in Table 1.

Table 1
Fracture criteria for a fully dense matrix or porous materials

Author(s)	Fracture criteria	
Freudenthal (1950)	$\int_0^{\bar{\varepsilon}_f} \bar{\sigma}\,\mathrm{d}\bar{\varepsilon} = C_1$	(11)
Cockcroft and Latham (1968)	$\int_0^{\bar{\varepsilon}_f} \bar{\sigma}\left(\frac{\sigma^*}{\bar{\sigma}}\right)\mathrm{d}\bar{\varepsilon} = C_2$	(12)
Brozzo et al. (1972)	$\int_0^{\bar{\varepsilon}_f} \frac{2\sigma^*}{3(\sigma^* - \sigma_h)}\,\mathrm{d}\bar{\varepsilon} = C_3$	(13)
Tabata and Masaki (1977)	$\int_0^{\bar{\varepsilon}_f} \left(A + \frac{\sigma_h}{\bar{\sigma}}\right)\mathrm{d}\bar{\varepsilon} = B \cdot \rho_{r_0}^C$	(14)

For the workability of a fully dense matrix, a critical constant of the generalized plastic work per unit of volume at fracture was introduced by Freudenthal [1], as expressed in Eq. (11), where $\bar{\sigma}$ is the effective stress, $\mathrm{d}\bar{\varepsilon}$ is the effective strain increment, $\bar{\varepsilon}_f$ is the effective strain at fracture, and C_1 is the critical constant for a matrix. However, this equation does not work in the compressive loading conditions.

Cockcroft and Latham [2] modified the criterion of the generalized plastic work by multiplying a nondimensional stress-concentration factor $\sigma^*/\bar{\sigma}$, as shown in Eq. (12), where σ^* is the largest tensile stress and C_2 is the critical constant. This equation recognizes the importance of the largest tensile stress at the crack initiation. If the compressive stress state exists in materials, $\sigma^* = 0$ is given in the criterion. Under this condition, the fracture will not occur in workpieces. In addition, the fracture criterion combining the level of both the largest tensile stress and the hydrostatic component was suggested by Brozzo et al. [3], and is shown in Eq. (13).

In consideration of the void influence on the forming limit of porous metals, Tabata and Masaki [15] proposed a criterion as presented in Eq. (14), where A, B, and C are the material constants and ρ_{r_0} is the initial relative density of a preform. This equation describes the effects of the hydrostatic stress on the fracture in porous materials; nevertheless, the constitution of void evolution is not taken into account.

3.2. Fracture mechanism

The forming limit in metalworking is a complex phenomenon that depends on both materials and deformation processes. We examine the fracture mechanism of porous metals to understand the workability. Generally, a failure occurs in materials under tensile loading. Observing the fracture mode in workpieces during deforming stage, we notice that the principal loading components dominate the initiation of a crack. The crack propagation is perpendicular to the first principal axis, which is determined by the first (maximum) principal stress at a point in materials.

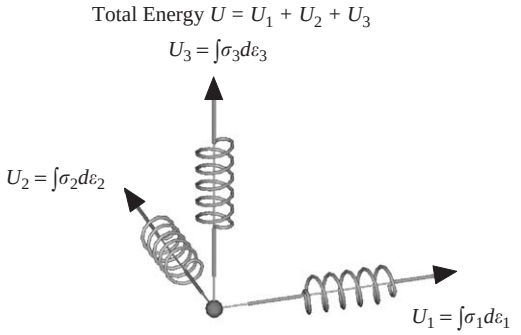

Fig. 2. The schematic diagram of the strain energy components on three principal axes.

Because of the plastic deformation in bulk forming problems, the strain energy density is adopted to describe the workability of materials. Inspired by the concept of the Cockcroft–Latham criterion for multiplying a nondimensional factor to emphasize the importance of the largest tensile stress at crack initiation, we focus on the strain energy densities on the principal axes. Any stress state can be uniquely described by stresses in the principal directions, in which the shear stresses are null. That is, the principal stresses with their directions can completely represent the stress state at a material point. By the same argument, the total strain energy density at a point can be similarly decomposed into three principal directions, in which each component is independent on the others. In order to demonstrate the concept, a schematic diagram of the strain energy components on the three principal axes is illustrated with a spring system as in Fig. 2. Since the principal directions of the stress and the strain state are consistent, each energy component can be expressed by integrating the principal stress and the corresponding principal strain. Consequently, the total strain energy density at a point can be decomposed into three components and is stated as follows:

$$U = U_1 + U_2 + U_3 = \int \sigma_1 \, \mathrm{d}\varepsilon_1 + \int \sigma_2 \, \mathrm{d}\varepsilon_2 + \int \sigma_3 \, \mathrm{d}\varepsilon_3, \tag{15}$$

where $\int \sigma_1 \, \mathrm{d}\varepsilon_1$ is the strain energy density on the first principal axis. Because the fracture is dominated by the first principal strain energy component, we can trace the ultimate value of $\int \sigma_1 \, \mathrm{d}\varepsilon_1$ to demonstrate the workability of materials.

3.3. New fracture criterion

The new fracture criterion for porous media is proposed adopting the strain energy density on the first principal axis, which is defined as the first principal strain energy density (FPSED). The effects of void evolution during deformation are considered as well. The new criterion is formulated with the following relation:

$$\int_0^{\varepsilon_{1fract}} \sigma_1 \, \mathrm{d}\varepsilon_1 = C_{cr} \cdot \mathrm{e}^{-mf}, \tag{16}$$

where σ_1 is the first (maximum) principal stress, $d\varepsilon_1$ is the corresponding principal strain increment, and ε_{1fract} is the first (maximum) principal strain at fracture; on the right-hand side of this equation, C_{cr} is the critical value for a fully dense matrix, and m is the material constant. The material constant m describes the sensitivity of the instantaneous void volume fraction, f, on the critical value of the FPSED for a medium. Fracture will occur once the accumulated FPSED at a material point meets the critical value. In particular, the increase of voids exponentially degrades the workability of porous metals. It is noted that the new forming-limit criterion can also be used to predict failure for the fully dense matrix as soon as f is reduced to zero. The critical constant of the matrix, C_{cr}, and the material parameter, m, in Eq. (16) are to be determined by experiment.

The new workability criterion for porous media is formulated based on the strain energy density in the first principal direction. In order to demonstrate the energy states of porous materials on the same basis, the principal strain energy densities in deformed bodies are modified by the factor e^{mf}, which denotes the compensation of void effects in materials. For this consideration, the new fracture criterion can be expressed as follows:

$$e^{mf} \cdot \int_0^{\varepsilon_{1fract}} \sigma_1 \, d\varepsilon_1 = C_{cr}. \tag{17}$$

Subsequently, we monitor $U_1 = e^{mf} \cdot \int \sigma_1 \, d\varepsilon_1$ in deformed bodies to evaluate the workability of porous materials, even if the first principal axis is changed by different loading conditions.

The new workability criterion is developed based on the critical value of the FPSED for a medium. In convenience of clarity, we demonstrate the new criterion in the plane-energy state, as shown in Fig. 3. By observing this figure, the modified strain energy density located in the down-left region of the critical boundary means what deformed bodies are safe. On the contrary, fracture occurs in materials once the modified principal strain energy density meets the critical value, C_{cr}. In addition, the dash line in the figure describes the symmetry of fracture locus on the energy plane.

The major contribution of this study is the development of a new fracture criterion for porous media to specifically include the mechanism of void evolution in the process. We verify the new workability criterion in the following analysis.

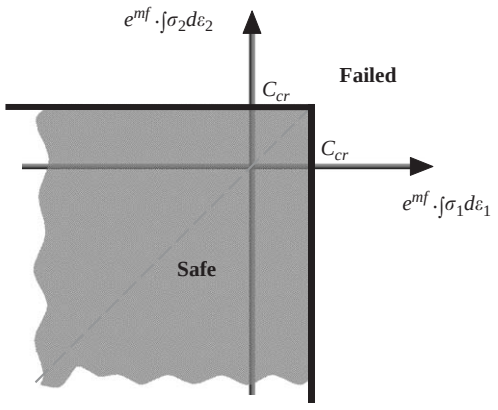

Fig. 3. The new fracture criterion in the state of the energy base.

4. Experimental work

4.1. Specimens preparation

The porous specimens used in the test are prepared from the water-atomized powder of iron. A variety of compacting pressures are utilized to obtain the cylindrical billets with different green densities and versatile aspect ratios. The compacted billets are measured as 12.5 mm in diameter, and the height is controlled by weight to ensure that the aspect ratio is less than 1.5 for preventing the specimens from buckling during compression. The floating die operation could enhance more homogeneous distribution of voids in the compacts.

The powder compacts are sintered in dry hydrogen at 1200 °C for 1 h and then cooled down in the furnace to the room temperature. In order to determine the mechanical properties of the matrix, some specimens are fully densified by rolling. The porous bulk is preheated at 1000 °C for enhancing the densification. In the rolling process, the roller is set as 2 revolutions per second. Since the microstructure plays a significant role on the plastic behavior, the process of recrystallization is applied in dry hydrogen at 600 °C for several minutes to dispel the work hardening induced by rolling. After recrystallization, the grain sizes in the matrix and the porous compacts are similar.

4.2. Uni-axial tension test of matrix

The material properties of the sintered materials are obtained from both the simple tension and the compression test, which are conducted using MTS 810 material testing system. In the uni-axial tension test of the matrix, the specimens are made of the fully densified sheets. They measure 50 mm in gauge length, 12.5 mm in width, and 2–3 mm in thickness. A strain gauge and an extensometer are used to monitor the deformation in the axial and transverse directions. Young's modulus, Poisson's ratio, the first yield stress, and plastic behavior of the matrix are also obtained. The tensile true stress–strain curve is demonstrated in Fig. 4. The plastic behavior of the matrix reveals a power law relation:

$$\bar{\sigma} = k(\bar{\varepsilon}_m^p)^n, \tag{18}$$

where the coefficient k is fitted at the value of 543.63 MPa and the strain hardening exponent n is about 0.3. The yield stress is found to be about 126 MPa.

4.3. Frictionless compression test of porous billets

For the frictionless upsetting, the porous billets with various initial densities and aspect ratios are tested. Teflon sheets are used as a lubricant at contact interfaces to maintain uniform deformation of these specimens under compressive loading. However, due to the compressibility of porous materials, the current cross-section of the billet during deformation cannot be determined through the incompressible volumetric plastic strain for a matrix in classical plasticity theory.

Based on the assumption of the homogeneous distribution of voids in billets, the average porosity evolution of each specimen can be measured with the total change of the volume in the

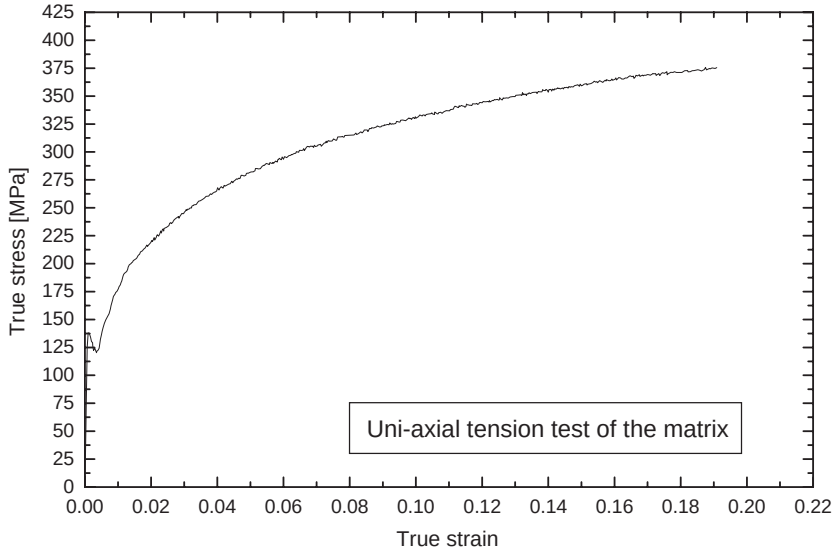

Fig. 4. The tensile true stress–strain curve of the fully dense matrix by experiment.

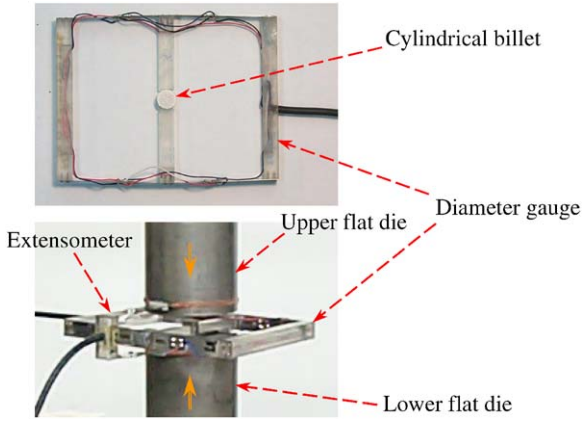

Fig. 5. The construction of the diameter gauge in the compression test.

frictionless upsetting. The diameter gauge, as shown in Fig. 5, is constructed to measure the dilated diameters of porous billets during compression. With the circular cross-section assumption and the diameter measured, the current area is calculated. Dividing the current area into the axial load, the true stress in the material is then obtained. Meanwhile, the instantaneous height of the billet is measured by extensometer. The void evolution is determined by the total change of the volume of the specimen. The volume is calculated by multiplying the current area and the instantaneous height.

The true stress–strain and true stress-porosity relations of the sintered compacts are obtained by frictionless compression. The details for determining the scalar parameters, q_1, q_2, and q_3, in

Table 2
The material constants

Matrix property			Porous parameter		
E (GPa)	v	$\sigma_{firstyield}$ (MPa)	q_1	q_2	q_3
180	0.27	126	1.81	1.00	2.80

the Gurson–Tvergaard equation are presented in our previous work [30]. The resulting values of Young's modulus, E, Poisson's ratio, v, the first yield stress of the matrix, $\sigma_{firstyield}$, and the scalar parameters of the porous metals are shown in Table 2.

4.4. Fracture upsetting test of porous billets

In addition to the frictionless test, upsetting experiments without Teflon sheets are carried out to perform the frictional effects and to determine the fracture strokes of the billets with various initial densities and at differing aspect ratios. Meanwhile, the load–displacement curves toward fracture are obtained. The fracture strokes of the porous compacts are then utilized to establish the forming-limit curve. After we accomplished these tests, the measured data are further investigated with the finite element analysis (FEA).

5. Finite element model verification

5.1. Basic assumptions

Bulk forming problems reflect the workability of materials. In fact, the material properties and the deformation characteristics are very complicated in real cases. In this study, some reasonable assumptions are made to simplify the analysis:

1. The matrix is perfectly bonded and incompressible.
2. The distribution of voids is homogeneous in the specimen.
3. The cylindrical billet is uniformly deformed during the frictionless upsetting.

In addition, we further assume that the change in void volume fraction is all brought about by the variation of existing voids and that the nucleation of new voids in the tensile stress state is negligible in this study.

5.2. Construction of finite element model

The commercial finite element program ABAQUS/Standard [31] is adopted to model and simulate the forging process of porous materials. The mesh and the boundary conditions of the cylindrical billet in the analysis of the open flat-die upsetting are demonstrated in Fig. 6. The

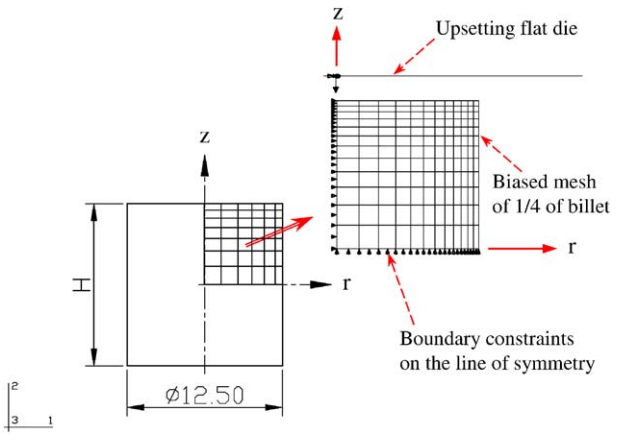

Fig. 6. Finite element mesh and boundary conditions of the billet in the upsetting analysis.

dimension of the billet is 12.5 mm in diameter, and the height depends on the tested specimen. Because of the axisymmetric profile, only one quarter of the billet and the die are modeled. The boundary constraints are specified on the line of symmetry. The discretization is biased toward the outward region to account for larger amounts of deformation and contact situations. The 4-node bilinear axisymmetric solid element is utilized for the billet, while the rigid surface is used for the flat die. The material parameters in Table 2 are input as well.

5.3. *Upsetting under frictionless and frictional conditions*

The standard Coulomb friction model is used to approximate the contact situations between the workpiece and the die. In order to verify the finite element results with the experiments, the upsetting simulation under different frictional conditions are considered. The coefficient of friction, μ, is given as zero in the frictionless analysis, in which the uniform deformation of billets is preserved. The results of frictionless upsetting simulation are used to examine whether the input data experimentally determined truly represents the actual bulk material behavior. Meanwhile, the upsetting analysis under frictional conditions is carried out to study the workability of porous materials.

In the frictionless upsetting, the compressive true stress–strain and true stress-porosity curves of the billets with 0.6897, 0.8071, and 0.9058 initial relative densities are demonstrated in Figs. 7 and 8. The results indicate that the finite element simulations closely match the measured data with only slight discrepancies. Fig. 7 shows that the yield strength and the loading capacity of the workpieces deteriorate with the presence of voids. In Fig. 8, the curves depict the void evolution in the frictionless upsetting. Since the finite element model is established based on the rigid-plastic formulation, the porosity in the specimen does not change in the elastic deformation. In order to precisely simulate the void evolution in the sintered preform during the plastic deformation, the relative density of the billet at the first yielding stage is given in the analysis. That is, the true stress-porosity curves by experiment and FEA are not starting with the same initial value of porosity.

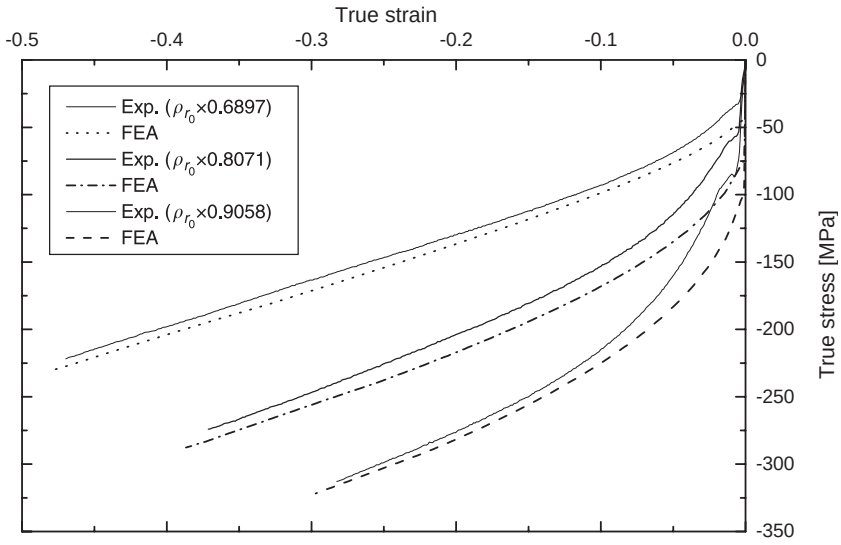

Fig. 7. Comparison of the true stress–strain curves in the frictionless upsetting of porous billets by experiment and FEA.

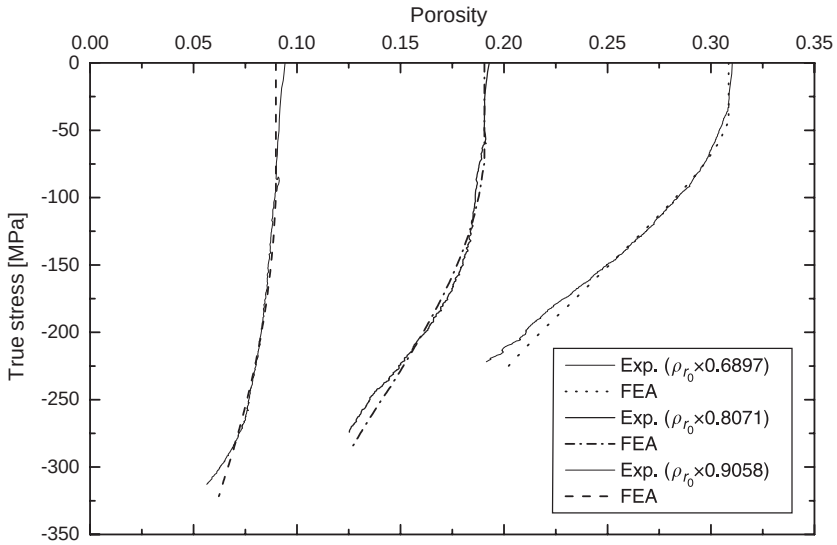

Fig. 8. Comparison of the stress–porosity curves toward fracture in the fractional upsetting of porous billets by experiment and FEA.

As another example of validation, the same upsetting process under frictional conditions is computed. The fracture upsetting simulation is carried out with an equivalent coefficient of friction, $\mu = 0.2$, which provides a similar bulged profile in the loading history to the specimen

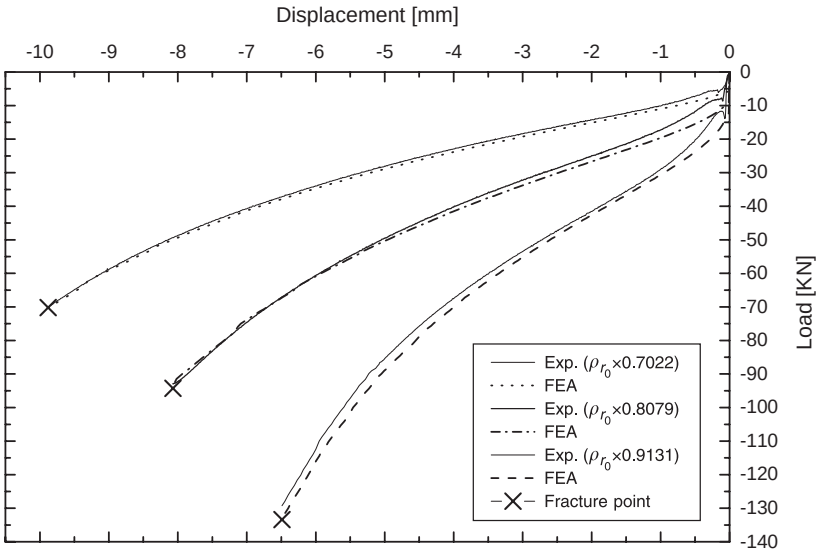

Fig. 9. Comparison of the load–displacement curves toward fracture in the fractional upsetting of porous billets by experiment and FEA.

from the experiment. The comparison of the load–displacement curves toward a crack initiation in the billets with 0.7022, 0.8079, and 0.9131 initial relative densities by experiment and FEA is illustrated in Fig. 9. It is clear that voids decrease the strength of the workpiece. Friction at contact interfaces of the billet and the flat die leads to non-uniform deformation and density variations, which cause the billet to bulge out and fracture on the equatorial surface. The fracture strokes of different billets are utilized to determine the critical value of the FPSED by finite element calculations.

5.4. Critical value of FPSED

5.4.1. User's subroutines

To execute the fracture prediction in the forging process, the user's subroutines USDFLD and URDFIL in ABAQUS are implemented in the model. The user's subroutines are empty. We can write the new forming-limit criterion for porous media in the subroutines. The procedure of the analysis that joins the user's subroutines is illustrated in Fig. 10. The FPSED in the material during deformation is calculated at each integration point by the user's subroutine USDFLD. The simulation will be terminated by the user's subroutine URDFIL as soon as the accumulated FPSED reaches the critical value in any time increment. This phenomenon suggests the fracture occurs in workpieces. Then, we can obtain the position of a crack initiation and the energy states in specimens by FEA.

5.4.2. Computation of FPSED

For the instances of the fracture-upsetting test in Fig. 9, the FPSED of billets with different initial relative densities and aspect ratios are exhibited in Table 3. The porosity at the crack point

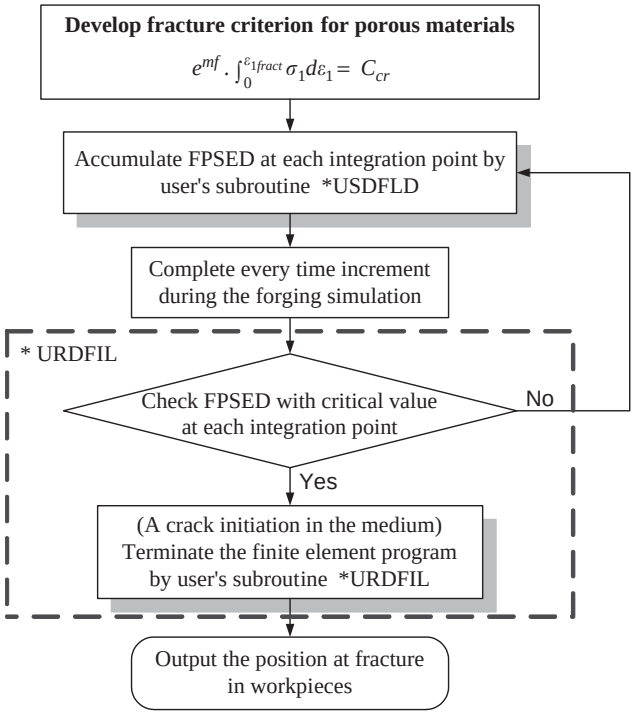

Fig. 10. Flow chart of the fracture prediction in the forging analysis with the user's subroutines USDFLD and URDFIL.

Table 3
The accumulated FPSED in the fracture-upsetting test of billets with different initial relative densities

Initial relative density	Height × diameter (mm × mm)	Fracture stroke (mm)	FPSED at fracture (MJ/m^3)	Porosity at fracture
0.7022	$18.79 \times \psi 12.50$	−9.8756	16.13 (Equat. surf.)	0.2073
0.8079	$15.55 \times \psi 12.51$	−8.0729	31.33 (Equat. surf.)	0.1426
0.9131	$11.92 \times \psi 12.52$	−6.4902	74.73 (Equat. surf.)	0.0742

in each specimen is shown as well. The increase of voids in materials reduces the FPSED at fracture. In addition to these values, the other 26 sets of the data conducted by the same procedure are demonstrated in Fig. 11. In evaluating the relations between the FPSED and the porosity at fracture, the exponential-decaying function is selected to fit these data. Thus, the forming-limit curve is established, where the critical value of the FPSED for the matrix, C_{cr}, is obtained as 179.77 and the material parameter, m, is equal to 12.59. This curve is implemented in the user's subroutines. As a result, the finite element model associated with the new workability criterion can be applied to predict fracture in P/F practices.

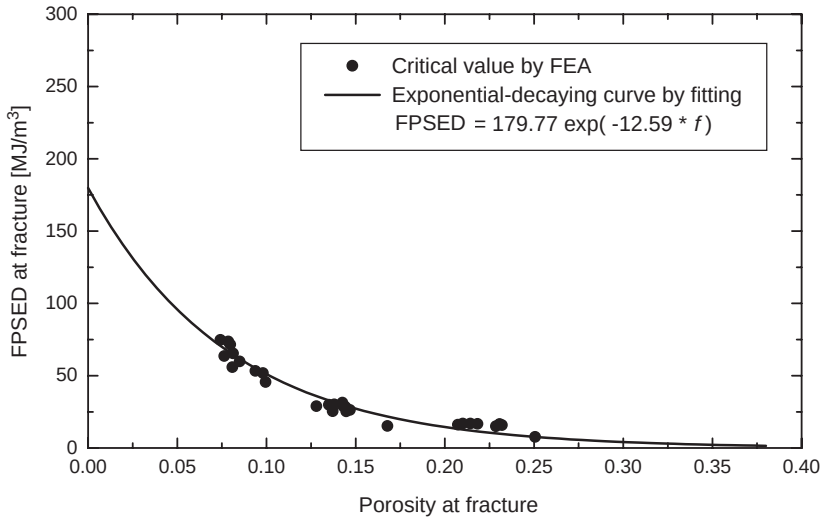

Fig. 11. The value of FPSED versus porosity at fracture and the exponential-decaying curve by fitting.

5.4.3. Results of fracture upsetting

The fracture upsetting analysis of sintered preforms is carried out with the new forgeability criterion. In order to compensate the void effects, the factor e^{mf} is multiplied to the principal strain energy densities in porous materials. For the instance of the fracture upsetting of the billet with 0.8079 initial relative densities, the modified principal strain energy densities at different points in the deformed body are demonstrated in Fig. 12. The data are observed under the line of symmetry, while most of them locate near the axes. The modified second principal strain energy density of each point on the bulge surface is insignificant. In particular, the modified FPSED, U_1, at the equator of the bulge billet, point K, meets the critical value of the matrix, C_{cr}, suggesting that fracture occurs at this point. The value of U_1 at point H is found to be close to the critical value. Furthermore, the directions of U_1 at points K, H, and G lie on the hoop axis. These data represent that a crack initiates on the equatorial surface and then propagates toward the contact sides, along with the direction perpendicularly to the circumference. This phenomenon is consistent with the picture of the fracture billet shown in Fig. 13.

For the energy state in the deformed billet shown in Fig. 12, the negative value of the principal strain energy component is caused by the opposite sign of the principal stress and the corresponding principal strain increment. Despite the minus principal energy components appear at several points, the total strain energy density, $U = U_1 + U_2 + U_3$, in all deformed bodies still have the positive value. Meanwhile, the value of U_1 is less than the third principal strain energy component, U_3, at most regions in the deformed billet. The results are contributed by the negative values of both the third (minimum) principal stress and the corresponding principal strain increment under compressive loading conditions. In other words, the FPSED does not always keep the maximum value among three principal energy components. In addition to these, the contours of the relative density in the deformed billet at fracture upsetting are shown in Fig. 13. The density variation occurs in the workpiece after large deformation, while the lowest value exists in the bulge region.

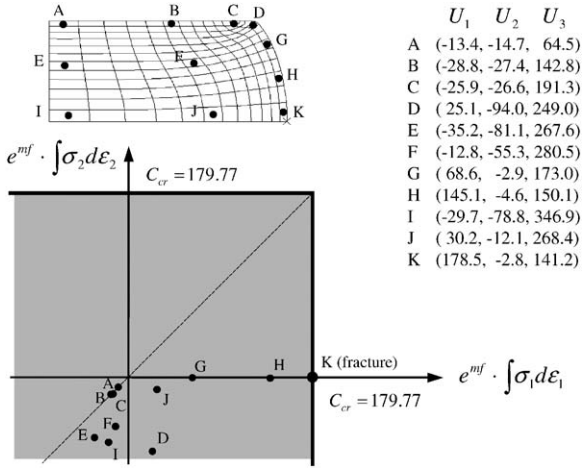

Fig. 12. The state of the modified principal strain energy densities at different points in the deformed billet with 0.8079 initial relative densities.

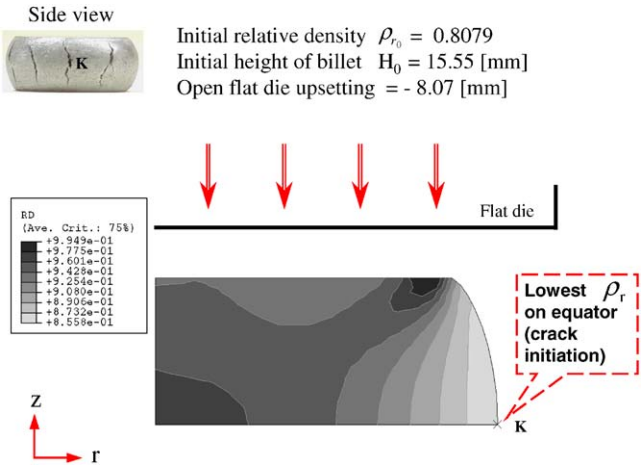

Fig. 13. Contours of the relative density in the billet at fracture upsetting.

5.4.4. *Comparison of different fracture criteria*

In the frictional upsetting simulation, the finite element model associated with the new fracture criterion truly represents the workability of sintered billets. Moreover, the comparisons of the strain energy densities at fracture points in the billets with various initial densities by different criteria are demonstrated in Table 4. In order to compensate the effects of porosity, the strain energy densities calculated by the first, second, and third criterion are modified by the factors $e^{m_1 f}$, $e^{m_2 f}$, and $e^{m_3 f}$, respectively. In these factors, m_1, m_2, and m_3 are the material parameters. The critical values of the modified strain energy densities, C_{cr1}, C_{cr2}, and C_{cr3}, in these criteria are obtained by the same procedure presented for C_{cr}.

Table 4
The modified strain energy densities at the fracture points in the billets with various initial relative densities by different criteria

Initial relative density	$e^{m_1 f} \cdot \int_0^{\bar{\varepsilon}_f} \bar{\sigma}\, \mathrm{d}\bar{\varepsilon}$	$e^{m_2 f} \cdot \int_0^{\bar{\varepsilon}_f} \bar{\sigma}\left(\frac{\sigma^*}{\bar{\sigma}}\right) \mathrm{d}\bar{\varepsilon}$	$e^{m_3 f} \cdot \int_0^{\bar{\varepsilon}_f} \left(A + \frac{\sigma_h}{\bar{\sigma}}\right) \mathrm{d}\bar{\varepsilon}$	$e^{mf} \cdot \int_0^{\varepsilon_{1\mathrm{fract}}} \sigma_1\, \mathrm{d}\varepsilon_1$
0.7022	927.76*	61.13	0.50	219.33
0.8079	786.92	56.61	0.50	188.65
0.9131	799.10	53.26	0.55	190.19
Critical value	$C_{\mathrm{cr1}} = 801.49$	$C_{\mathrm{cr2}} = 51.04$	$C_{\mathrm{cr3}} = 0.55$	$C_{\mathrm{cr}} = 179.77$
Material const.	$m_1 = 3.42$	$m_2 = 7.46$	$m_3 = 0.21$	$m = 12.59$
Crack point	Upper corner	Equat. surf.	Upper corner	Equat. surf.

*Unit: ($\mathrm{MJ/m^3}$).

It can be observed that the modified strain energy densities are similar to the critical value in the same criterion. In particular, the crack point on the equatorial surface, which is presented by the second and fourth criterion, is consistent with the experiment. The fourth equation, the new fracture criterion, is formulated by the strain energy density on the first principal axis. Meanwhile, the second formula is established by multiplying the generalized plastic work and a stress-concentration factor $\sigma^*/\bar{\sigma}$. If the compressive stress state exists in materials, $\sigma^* = 0$ is given in the criterion. Nevertheless, the accumulated strain energy density is not the true value in deformed materials. This criterion may not precisely predict fracture in workpieces under complex loading conditions. In addition, the position of the crack initiation is misled by the first and the third criterion, which are comprised of the effective stress and the hydrostatic component. For this discussion, the fracture upsetting simulation by applying the new workability criterion demonstrates much better accuracy than the results derived from the equations proposed by other researchers.

6. Fracture prediction in powder forging practice

6.1. Finite element model construction

The fracture prediction in forging a gear blank as one exercise of P/F applications by using the verified finite element model is performed. In the practice of forging the gear blank, the profiles of the preform and the die are illustrated in Fig. 14. The billet is 6 mm in height and 12.5 mm in diameter, and the die is 27.5 mm in diameter. The 4-node bilinear axisymmetric solid element is used for the billet, and the 2-node linear axisymmetric rigid element is utilized to construct the die in the finite element model. Because of the axisymmetric profile, only one quarter of the billet and the die are modeled. The boundary conditions are specified on the line of symmetry. The discretization is made finer in the middle region of the billet to precisely account for larger amounts of deformation. The material parameters in Table 2 are input as well.

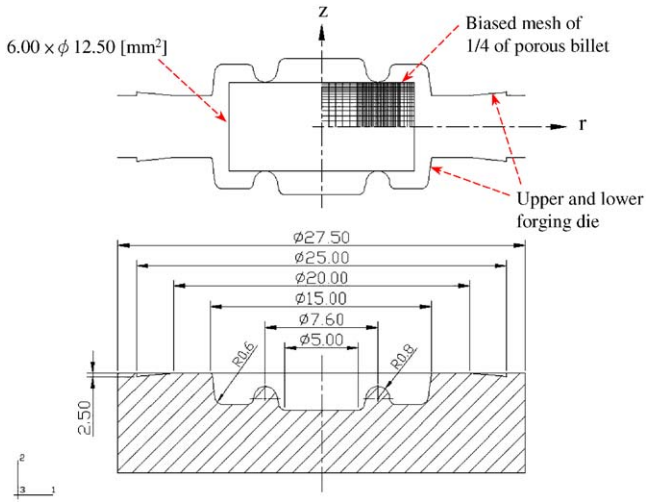

Fig. 14. Profiles of the preform and the die in forging the gear blank.

6.2. Fracture prediction in forging process

In the forging analysis, the coefficient of friction, μ, is approximated as 0.2 to deal with the complicated contact situations. In order to investigate the void effects on the forgeability, the preforms with about 0.7, 0.8, and 0.9 initial relative densities are prepared. The comparison of the forging load-stroke curves toward crack initiation in the workpiece by experiment and FEA is demonstrated in Fig. 15. The forging load and the stroke at fracture are reduced by the increase of voids in the preform.

Taking the forging simulation of the preform with about 0.8 initial relative densities, for example, the state of the modified principal strain energy densities at different points in the workpiece are demonstrated in Fig. 16. Most of the data locate under the line of symmetry. In particular, the modified FPSED, U_1, at point B meets the critical value, C_{cr}, suggesting that a fracture occurs on the top-inner surface of the workpiece. Furthermore, the crack initiates on the circumference, for the direction of U_1 at point B lies on the radial axis. This phenomenon is consistent with the picture of the fracture workpiece shown in Fig. 17.

Observing the data in Fig. 16, the values of U_1 at points B′, B″, and D are found to be close to the critical value. Meanwhile, the U_1 at the point on the top surface of the workpiece is larger than the other two principal strain energy densities. For the element in the tensile stress state, the FPSED has the maximum value among three principal energy components. Although the minus principal strain energy components appear at several points in the workpiece, the total strain energy density, $U = U_1 + U_2 + U_3$, in all deformed bodies still keep the positive value. In addition to these, the distributions of the relative density in the workpiece at fracture forging are shown in Fig. 17. The lowest density appears in the top-inner region, where the largest value of U_1 exists. The fracture prediction in forging the gear blank by FEA is validated by the experiment.

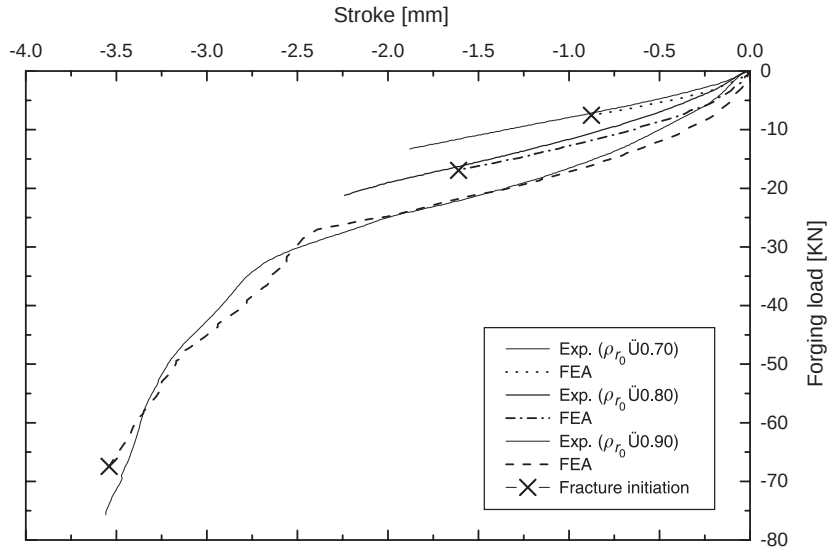

Fig. 15. Comparison of the forging load–stroke curves toward crack initiation in the workpiece by experiment and FEA.

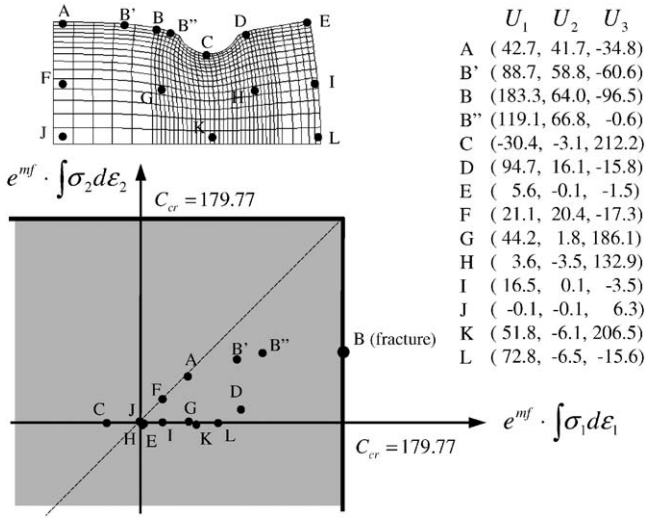

Fig. 16. The state of the modified principal strain energy densities at different points in the workpiece with about 0.8 initial relative densities.

7. Conclusions

P/F technique enhances the dimension precision and the strength of products. Forging simulations help better understanding of the workability of sintered preforms. The major

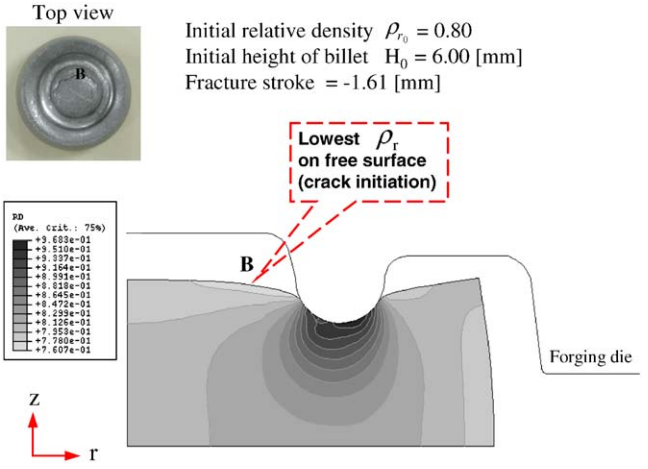

Fig. 17. Contours of the relative density in the workpiece at fracture forging.

contribution of this investigation is the fracture prediction in P/F practices by developing a new forming-limit criterion for porous media to include the mechanism of void evolution. Based on the results of this research, the following conclusions are drawn:

(1) The fracture simulation in P/F practices, verified with experiments, is achieved by using the new forming-limit criterion for porous media.
(2) The new workability criterion for porous metals is formulated with the strain energy density on the first principal axis, which is defined as the FPSED.
(3) By applying this new criterion, the fracture upsetting simulation demonstrates much better accuracy than the results derived from the equations proposed by other researchers.
(4) Besides the degradation of the strength, this study specifically shows that voids in the sintered preform exponentially reduce the forging limit.

Through the computer simulation of the forging limits of porous materials with the new fracture criterion, we can then predict a fracture even in complex forging applications, such as connecting rods, ratchet wheels, etc. Such capability would be helpful in optimizing the geometry of sintered preforms and forging dies.

Acknowledgments

The authors acknowledge the generous support of experimental facilities from Prof. Kuen-Shyang Hwang of the Department of Materials Science and Engineering, Natioanl Taiwan University. This research was sponsored by the National Science Council of the Republic of China under Grant No. NSC 90-2212-E-002-171.

References

[1] Freudenthal AM. The inelastic behaviour of solids. New York, USA: Wiley; 1950.
[2] Cockcroft MG, Latham DJ. Ductility and the workability of metals. Journal of the Institute of Metals 1968;96:33–9.
[3] Brozzo P, Deluca B, Rendina R. A new method for the prediction of formability limits in metal sheets. Sheet metal forming and formability; Proceedings of the seventh biannual conference of International Deep Drawing Research Group, 1972.
[4] Norris D, Reaugh J, Moran B, Quinnonesa D. A plastic strain mean-stress criterion for ductile fracture. Journal of Engineering Materials and Technology, Transactions of the ASME 1978;100:279–86.
[5] Oyane M, Sato T, Okimoto K, Shima S. Criteria for ductile fracture and their applications. Journal of Mechanical and Working Technology 1980;4:65–81.
[6] Clift SE, Hartley P, Sturgess CEN, Rowe GW. Fracture prediction in plastic deformation processes. International Journal of Mechanical Sciences 1990;32:1–17.
[7] Gouveia BPPA, Rodrigues JMC, Martins PAF. Fracture predicting in bulk metal forming. International Journal of Mechanical Sciences 1996;38:361–72.
[8] Gouveia BPPA, Rodrigues JMC, Martins PAF. Ductile fracture in metalworking: experimental and theoretical research. Journal of Materials Processing Technology 2000;101:52–63.
[9] Wifi AS, Abdel-Hamid A, El-Abbasi N. Computer-aided evaluation of workability in bulk forming processes. Journal of Materials Processing Technology 1998;77:285–93.
[10] Jain M, Allin J, Lloyd DJ. Fracture limit prediction using ductile fracture criteria for forming of an automotive aluminum sheet. International Journal of Mechanical Sciences 1999;41:1273–88.
[11] Takuda H, Mori K, Hatta N. The application of some criteria for ductile fracture to the prediction of the forming limit of sheet metals. Journal of Materials Processing Technology 1999;95:116–21.
[12] Abdel-Rahman M, El-Sheikh MN. Workability in forging of powder metallurgy compacts. Journal of Materials Processing Technology 1995;54:97–102.
[13] Downey CL, Kuhn HA. Application of a forming limit concept to the design of powder preforms for forging. Journal of Engineering Materials and Technology, Transactions of the ASME 1975;97:121–5.
[14] Zhang XQ, Peng YH, Li MQ, Wu SC, Ruan XY. Study of workability limits of porous materials under different upsetting conditions by compressible rigid plastic finite element method. Journal of Materials and Engineering Performance 2000;9:164–9.
[15] Tabata T, Masaki S. A fracture criterion for porous materials and its application to the shape of sintered preforms in forging. Journal of Engineering Materials and Technology, Transactions of the ASME 1977;99:16–22.
[16] Lee JH, Zhang Y. A finite-element work-hardening plasticity model of the uniaxial compression and subsequent failure of porous cylinders including effects of void nucleation and growth—Part II: Localization and fracture criteria. Journal of Engineering Materials and Technology, Transactions of the ASME 1996;118:169–78.
[17] McClintock FA. A criterion for ductile fracture by the growth of holes. Journal of Applied Mechanics, Transactions of the ASME 1968;35:363–71.
[18] Roy GL, Embury JD, Edward G, Ashby MF. A model of ductile fracture based on the nucleation and growth of voids. Acta Metallurgica 1981;29:1509–22.
[19] Sowerby R, Chandrasekaran N. The prediction of damage accumulation when upsetting AISI 1045 steel specimens, based on McClintock's model. Materials Science and Engineering A 1986;79:27–35.
[20] Spitzig WA, Smelser RE, Richmond O. The evolution of damage and fracture in iron compacts with various initial porosity. Acta Metallurgica 1988;36:1201–11.
[21] Spitzig WA. Effect of hydrostatic pressure on deformation, damage evolution, and fracture of iron with various initial porosity. Acta Metallurgica et Materialia 1990;38:1445–53.
[22] Gurson AL. Plastic flow and fracture behavior of ductile materials incorporating void nucleation, growth and interaction. Ph.D. Dissertation, Brown University, 1975.
[23] Gurson AL. Continuum theory of ductile rupture by void nucleation and growth: Part I—Yield criteria and flow rules for porous ductile media. Journal of Engineering Materials and Technology, Transactions of the ASME 1977;99:2–15.

[24] Tvergaard V. Influence of voids on shear band instabilities under plane strain conditions. International Journal of Fracture 1981;17:389–407.
[25] Goods SH, Brown LM. The nucleation of cavities by plastic deformation. Acta Metallurgica 1979;27:1–15.
[26] Chu CC, Needleman A. Void nucleation effects in biaxially stretched sheets. Journal of Engineering Materials and Technology, Transactions of the ASME 1980;102:249–56.
[27] Hom CL, McMeeking RM. Void growth in elastic–plastic materials. Journal of Applied Mechanics, Transactions of the ASME 1989;56:309–17.
[28] Lee JH, Zhang Y. A finite-element work-hardening plasticity model of the uniaxial compression and subsequent failure of porous cylinders including effects of void nucleation and growth—Part I: Plastic flow and damage. Journal of Engineering of Materials and Technology, Transactions of the ASME 1994;116:69–79.
[29] Yi S. Influence of void nucleation and growth on deformation localization in tensile sheet specimen. Engineering of Fracture Mechanics 1995;51:381–9.
[30] Huang CC, Cheng JH. Forging simulation of sintered powder compacts under various frictional conditions. International Journal of Mechanical Sciences 2002;44:489–507.
[31] Hibbit J, Karlsson, Sorensen P. ABAQUS/standard user's manual, version 5.8. RI, USA: Hibbit, Karlsson & Sorensen Inc.; 2000.